

Shape of Motion: 4D Reconstruction from a Single Video

Qianqian Wang^{1,2*}, Vickie Ye^{1*}, Hang Gao^{1*},
Jake Austin¹, Zhengqi Li², and Angjoo Kanazawa¹

¹ UC Berkeley ² Google Research

Abstract. Monocular dynamic reconstruction is a challenging and long-standing vision problem due to the highly ill-posed nature of the task. Existing approaches are limited in that they either depend on templates, are effective only in quasi-static scenes, or fail to model 3D motion explicitly. In this work, we introduce a method capable of reconstructing generic dynamic scenes, featuring explicit, full-sequence-long 3D motion, from casually captured monocular videos. We tackle the under-constrained nature of the problem with two key insights: First, we exploit the low-dimensional structure of 3D motion by representing scene motion with a compact set of $\mathbb{SE}(3)$ motion bases. Each point’s motion is expressed as a linear combination of these bases, facilitating soft decomposition of the scene into multiple rigidly-moving groups. Second, we utilize a comprehensive set of data-driven priors, including monocular depth maps and long-range 2D tracks, and devise a method to effectively consolidate these noisy supervisory signals, resulting in a globally consistent representation of the dynamic scene. Experiments show that our method achieves state-of-the-art performance for both long-range 3D/2D motion estimation and novel view synthesis on dynamic scenes. Project Page: shape-of-motion.github.io

Keywords: Long-range 3D motion tracking · Monocular dynamic novel view synthesis · 4D Reconstruction

1 Introduction

Reconstructing the persistent geometry and their 3D motion across a video is crucial for understanding and interacting with the underlying physical world. While recent years have seen impressive progress in modeling static 3D scenes [39, 61], recovering the geometry and motion of complex dynamic 3D scenes, especially from a single video, remains an open challenge. A number of prior dynamic reconstruction and novel view synthesis approaches have attempted to tackle this problem. However, most methods rely on synchronized multi-view videos [8, 19, 19, 58, 99] or additional LIDAR/depth sensors [24, 55, 68, 91, 97]. Recent monocular approaches can operate on regular dynamic videos, but they typically model

* Equal Contribution

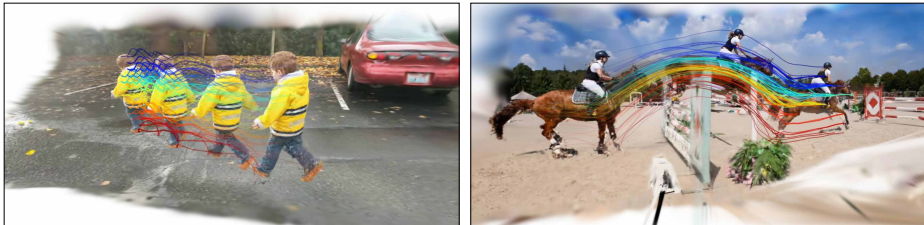


Fig. 1: Shape of Motion. Our approach enables joint 3D long-range tracking and novel view synthesis from a monocular video of a complex dynamic scene. Here, we demonstrate our ability to render moving scene elements at fixed viewpoint with different moments in time. Additionally, we visualize the estimated long-range 3D motion as colorful trajectories. These trajectories reveal distinct geometric patterns that encapsulate the movement of each point through 3D space and time, which leads us to the term “Shape of Motion”.

3D scene motion as short-range scene flow between consecutive times [20, 51, 52] or deformation fields that maps between canonical and view space [64, 65, 108], failing to capture 3D motion trajectories persistent over a video.

The longstanding challenge for more general in-the-wild videos lies in the poorly constrained nature of the reconstruction problem. In this work, we tackle this challenge with two key insights. The first is that, while the image space dynamics can be complex and discontinuous, the underlying 3D motion is a composition of continuous simple rigid motions. Our second insight is that data-driven priors provide complementary, though noisy cues, that aggregate well into a globally coherent representation of the 3D scene geometry and motion.

Motivated by these two insights, we represent the dynamic scene as a set of persistent 3D Gaussians, and represent their motion across the video in terms of a compact set of shared $\text{SE}(3)$ motion bases. Unlike traditional scene flow, which computes 3D correspondence between consecutive frames, our representation recovers a persistent 3D trajectory over the whole video, enabling long-range 3D tracking. As the 3D trajectories produced by our method capture the geometric patterns that trace each point’s movement through 3D space and time, we refer to our approach “Shape of Motion”, as shown in Figure 1. We show how to fit our explicit scene representation to a general video in-the-wild, by fusing together complementary cues from two main sources: monocular depth estimates per-frame, and 2D track estimates across frames. We conduct extensive evaluations on both synthetic and real-world dynamic video datasets, and show that our proposed approach significantly outperforms prior monocular dynamic novel view synthesis methods and 3D tracking baselines in both long-range 2D and 3D tracking accuracy. Moreover, we achieve state-of-the-art novel view synthesis quality among all existing methods. In summary, our key contributions include: (1) A new dynamic scene representation enabling both real-time novel view synthesis and globally consistent 3D tracking for any point at any time. (2) A carefully designed framework that optimizes the representation on posed monocular video by leveraging physical motion priors and data-driven priors.

2 Related Work

Correspondences and Tracking. Monocular 3D long-range tracking has not been explored broadly in the literature, but there exist many approaches to perform tracking in 2D image space. A typical way for determining 2D point correspondences relies on optical flows. This involves estimating dense motion fields between image pairs [4, 6, 7, 9, 15, 27, 28, 28, 31, 35–37, 57, 71, 79, 85, 86, 101]. While effective for consecutive frames, accurate long-term tracking in videos remains a challenge with optical flow methods. Sparse keypoint matching methods can enable long trajectory generation [2, 12, 53, 56, 73], but these methods are primarily intended for sparse 3D reconstruction. Long-range 2D trajectory estimation for arbitrary points has been explored in earlier works, which relied on hand-crafted priors to generate motion trajectories [3, 72, 75, 76, 80, 92]. Recently, there has been a resurgence of interest in this problem, with several works showcasing impressive long-term 2D tracking results on challenging, in-the-wild videos. These approaches employ either test-time optimization where models consolidate noisy short-range motion estimates into a global representation for producing long-term correspondences [62, 94], or data-driven strategies [14, 25, 38], where neural networks learn long-term correspondence estimates from synthetic data [13, 112]. While these methods effectively track any 2D point throughout a video, they lack the knowledge of underlying 3D scene geometry and motions.

Scene flow or 3D motion trajectory is a common representation to model 3D scene motion and point correspondences. Most prior work estimates scene flow directly from Lidar point clouds [24, 55, 68, 91, 97] or RGBD images [34, 60, 69, 84, 88, 89]. In monocular setting, a few recent works proposed to estimate 3D motions through self-supervised learning or test-time optimization strategies [30, 51, 52, 102–104], but these approaches either focus on a single object, require template priors, or only produce short-range motion correspondences. In contrast, our method does not rely on template priors and is capable of producing long-range 3D trajectories, making it suitable for modeling complex scenes with multiple moving objects.

Dynamic Reconstruction and View Synthesis. Our work also relates to dynamic 3D scene reconstruction and novel view synthesis problems. In non-rigid reconstruction, early methods often required RGBD sensors [5, 16, 32, 63, 113] or strong hand-crafted priors [45, 70, 74]. Recent work has demonstrated progress toward the reconstruction of dynamic scenes in the wild by integrating monocular depth priors [43, 50, 59, 110, 111]. Recently, Neural Radiance Fields (NeRF) [61] and Gaussian Splat [40] based approaches have achieved state-of-the-art results. Most of these methods [1, 8, 10, 19, 19, 48, 49, 81, 83, 93] require simultaneous multi-view video observations or predefined templates [33, 47, 98] for high-quality novel view outputs. Template-free monocular approaches model dynamic scenes with different types of representations such as video depth maps [109], time-dependent NeRFs [17, 51, 52, 64, 65, 67, 90, 100], and dynamic 3D Gaussians [18, 99, 107, 108]. While significant progress has been made, as DyCheck [21] pointed out, many

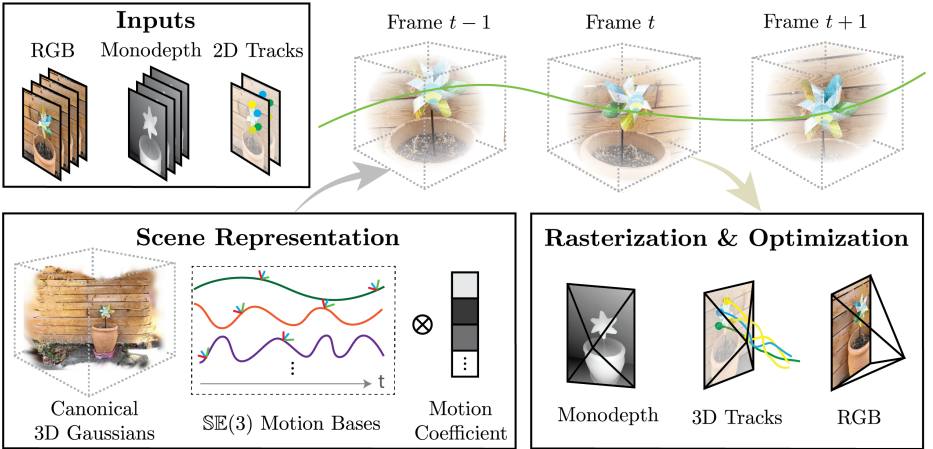


Fig. 2: System Overview. Given a single RGB video sequence with known camera poses, along with monocular depth maps and 2D tracks computed from off-the-shelf models [14, 106] as input, we optimize a dynamic scene representation as a set of persistent 3D Gaussians that translate and rotate over time. To capture the low-dimensional nature of scene motion, we model the motion with a set of compact $\text{SE}(3)$ motion bases shared across all scene elements. Each 3D Gaussian’s motion is represented as a linear combination of these global $\text{SE}(3)$ motion bases, weighted by motion coefficients specific to each Gaussian. We supervise our scene representation (canonical 3D Gaussian parameters, per-Gaussian motion coefficients, and global motion bases) by comparing the rendered outputs (RGB, depths and 2D tracks) with the corresponding input signals. This results in a dynamic 3D representation of the scene with explicit long-range 3D scene motion.

approaches focus on scenarios with camera teleportation [44, 108] or quasi-static scenes, which do not represent real-world monocular videos. In this work, we focus on modeling casual videos captured by a single camera, a more practical and challenging setup.

3 Method

Our method takes as input a sequence of T video frames $\{I_t \in \mathbb{R}^{H \times W \times 3}\}$ of a dynamic scene, the camera intrinsics $\mathbf{K}_t \in \mathbb{R}^{3 \times 3}$, and world-to-camera extrinsics $\mathbf{E}_t \in \text{SE}(3)$ of each input frame I_t . From these inputs, we aim to recover the geometry of the entire dynamic scene and the full-length 3D motion trajectory of every point in the scene. Unlike most prior dynamic NeRFs methods [21, 50, 52, 90, 100] which render the scene contents through volumetric ray casting and represent the motion implicitly at fixed 3D locations, we model the dense scene elements as a set of canonical 3D Gaussians, but allow them to translate and rotate over entire video through full-length motion trajectories. We adopt explicit point-based representation because it simultaneously allows for both (1)

high-fidelity rendering in real-time and (2) full-length 3D tracking of any surface point from any input time.

Optimizing an explicit representation of dynamic 3D Gaussians from a single video is severely ill-posed – at each point in time, the moving subjects in the scene are observed at those poses from only a single viewpoint. In order to overcome this ambiguity, we make two insights: First, we note that, while the projected 2D dynamics might be complex in the video, the underlying 3D motion in the scene is low-dimensional, and composed of simpler units of rigid motion. Second, powerful data-driven priors, namely monocular depth estimates and long-range 2D tracks, provide complementary but noisy signals of the underlying 3D scene. We propose a system that allows us to fuse these noisy estimates together into a globally coherent representation of both the scene geometry and motion.

The following sections introduce our framework. We represent the scene contents as a globally consistent set of 3D Gaussians that live in a canonical space (Section 3.1). To recover consistent motion trajectories, we bind the 3D Gaussians to a compact and low-dimensional motion parameterization. In particular, we represent the full-length motion trajectories of each dynamic scene element with a set of compact and low-dimensional $\text{SE}(3)$ motion bases (Section 3.2). Finally, we fit these motion bases to the input video frames, constraining our optimization with structural priors and data-driven priors (Section 3.3). We show a schematic of our pipeline in Figure 2.

3.1 Preliminaries: 3D Gaussian Splatting

We represent the appearance and geometry of dynamic scene contents with a global set of 3D Gaussians, an explicit and expressive differentiable scene representation [39] for efficient optimization and rendering. We define parameters of each 3D Gaussian in the canonical frame t_0 as $\mathbf{g}_0 \equiv (\boldsymbol{\mu}_0, \mathbf{R}_0, \mathbf{s}, o, \mathbf{c})$, where $\boldsymbol{\mu}_0 \in \mathbb{R}^3$, $\mathbf{R}_0 \in \text{SO}(3)$ are the 3D mean and orientation in the canonical frame, and $\mathbf{s} \in \mathbb{R}^3$ the scale, $o \in \mathbb{R}$ the opacity, and $\mathbf{c} \in \mathbb{R}^3$ the color, are persistent properties shared across time. To render a set of 3D Gaussians from a camera with world-to-camera extrinsics \mathbf{E} and intrinsics \mathbf{K} , the projections of the 3D Gaussians in the image plane are obtained by 2D Gaussians parameterized as $\boldsymbol{\mu}'_0 \in \mathbb{R}^2$ and $\boldsymbol{\Sigma}'_0 \in \mathbb{R}^{2 \times 2}$ via affine approximation

$$\boldsymbol{\mu}'_0(\mathbf{K}, \mathbf{E}) = \Pi(\mathbf{K}\mathbf{E}\boldsymbol{\mu}_0) \in \mathbb{R}^2, \quad \boldsymbol{\Sigma}'_0(\mathbf{K}, \mathbf{E}) = \mathbf{J}_{\mathbf{K}\mathbf{E}}\boldsymbol{\Sigma}_0\mathbf{J}_{\mathbf{K}\mathbf{E}}^\top \in \mathbb{R}^{2 \times 2}, \quad (1)$$

where Π is perspective projection, and $\mathbf{J}_{\mathbf{K}\mathbf{E}}$ is the Jacobian of perspective projection with \mathbf{K} and \mathbf{E} at the point $\boldsymbol{\mu}_0$. The 2D Gaussians can then be efficiently rasterized into RGB image and depth map via alpha compositing as

$$\hat{\mathbf{I}}(\mathbf{p}) = \sum_{i \in H(\mathbf{p})} T_i \alpha_i \mathbf{c}_i, \quad \hat{\mathbf{D}}(\mathbf{p}) = \sum_{i \in H(\mathbf{p})} T_i \alpha_i \mathbf{d}_i, \quad (2)$$

where $\alpha_i = o_i \cdot \exp(-\frac{1}{2}(\mathbf{p} - \boldsymbol{\mu}'_0)^T \boldsymbol{\Sigma}'_0 (\mathbf{p} - \boldsymbol{\mu}'_0))$, and $T_i = \prod_{j=1}^{i-1} (1 - \alpha_j)$. $H(\mathbf{p})$ is the set of Gaussians that intersect the ray shoot from the pixel \mathbf{p} . This process is fully differentiable, and enables direct optimization of the 3D Gaussian parameters.

3.2 Dynamic Scene Representation

Scene Motion Parameterization. To model a dynamic 3D scene, we keep track of N canonical 3D Gaussians and vary their positions and orientations over time with a per frame rigid transformation. In particular, for a moving 3D Gaussian at time t , its pose parameters $(\boldsymbol{\mu}_t, \mathbf{R}_t)$ are rigidly transformed from the canonical frame t_0 to t via $\mathbf{T}_{0 \rightarrow t} = [\mathbf{R}_{0 \rightarrow t} \mathbf{t}_{0 \rightarrow t}] \in \mathbb{SE}(3)$:

$$\boldsymbol{\mu}_t = \mathbf{R}_{0 \rightarrow t} \boldsymbol{\mu}_0 + \mathbf{t}_{0 \rightarrow t}, \quad \mathbf{R}_t = \mathbf{R}_{0 \rightarrow t} \mathbf{R}_0. \quad (3)$$

Rather than modeling the 3D motion trajectories independently for each Gaussian, we define a set of $B \ll N$ learnable basis trajectories $\{\mathbf{T}_{0 \rightarrow t}^{(b)}\}_{b=1}^B$ that are globally shared across all Gaussians [44]. The transformation $\mathbf{T}_{0 \rightarrow t}$ at each time t is then computed by a weighted combination of this global set of basis trajectories through per-point basis coefficients $\mathbf{w}^{(b)}$ via

$$\mathbf{T}_{0 \rightarrow t} = \sum_{b=0}^B \mathbf{w}^{(b)} \mathbf{T}_{0 \rightarrow t}^{(b)}, \quad (4)$$

where $\|\mathbf{w}^{(b)}\| = 1$. In our implementation, we parameterize $\mathbf{T}_{0 \rightarrow t}^{(b)}$ as 6D rotation [26] and translation, and perform the weighted combination separately on each with the same weight $\mathbf{w}^{(b)}$. During optimization, we jointly learn the set of global motion bases and motion coefficients of each 3D Gaussian. These compact motion bases explicitly regularize the trajectories to be low-dimensional, encouraging the 3D Gaussians that move similarly to each other to be represented by similar motion coefficients.

Rasterizing 3D trajectories. Given this representation, we now describe how we obtain pixelwise 3D motion trajectory at any query frame I_t . we take a similar approach to Wang *et al.* [94] and rasterize the motion trajectories of 3D Gaussians into query frame I_t . Namely, for a query camera at time t with intrinsics \mathbf{K}_t and extrinsics \mathbf{E}_t , we perform rasterization to obtain a map ${}^w\hat{\mathbf{X}}_{t \rightarrow t'} \in \mathcal{R}^{H \times W \times 3}$ that contains the expected 3D world coordinates of the surface points corresponding to each pixel at target time t'

$${}^w\hat{\mathbf{X}}_{t \rightarrow t'}(\mathbf{p}) = \sum_{i \in H(\mathbf{p})} T_i \alpha_i \boldsymbol{\mu}_{i,t'}, \quad (5)$$

where $H(\mathbf{p})$ is the set of Gaussians that intersect the pixel \mathbf{p} at query time t . The 2D correspondence location at time t' for a given pixel \mathbf{p} , $\hat{\mathbf{U}}_{t \rightarrow t'}(\mathbf{p})$, and the corresponding depth value at time t' , $\hat{\mathbf{D}}_{t \rightarrow t'}(\mathbf{p})$ can then be written as

$$\hat{\mathbf{U}}_{t \rightarrow t'}(\mathbf{p}) = \Pi(\mathbf{K}_{t'} {}^c\hat{\mathbf{X}}_{t \rightarrow t'}(\mathbf{p})), \quad \hat{\mathbf{D}}_{t \rightarrow t'}(\mathbf{p}) = ({}^c\hat{\mathbf{X}}_{t \rightarrow t'}(\mathbf{p}))_{[3]} \quad (6)$$

where ${}^c\hat{\mathbf{X}}_{t \rightarrow t'}(\mathbf{p}) = \mathbf{E}_{t'} {}^w\hat{\mathbf{X}}_{t \rightarrow t'}(\mathbf{p})$, Π is a perspective projection operation, and $(\cdot)_{[3]}$ is the third element of a vector.

3.3 Optimization

We prepare the following estimates using off-the-shelf methods in our optimization: 1) masks for the moving objects for each frame $\{\mathbf{M}_t\}$, which can be easily obtained using Track-Anything [42, 105] with a few user clicks, 2) monocular depth maps $\{\mathbf{D}_t\}$ computed using state-of-the-art relative depth estimation method Depth Anything [106] and 3) long-range 2D tracks $\{\mathbf{U}_{t \rightarrow t'}\}$ for foreground pixels from state-of-the-art point tracking method TAPIR [14]. We align the relative depth maps with the metric depth maps by computing a per-frame global scale and shift and use them for our optimization, as we found relative depth maps tend to contain finer details. We treat the lifted 2D tracks unprojected with the aligned depth maps as noisy initial 3D track observations $\{\mathbf{X}_t\}$ for the moving objects. For the static part of the scene, we model them using standard static 3D Gaussians and initialize their 3D locations by unprojecting them into the 3D space using the aligned depth maps. The static and dynamic Gaussians are jointly optimized and rasterized together to form an image. We focus on describing the optimization process for dynamic Gaussians below.

Initialization. We first select the canonical frame t_0 to be the frame in which the most 3D tracks are visible, and initialize the Gaussian means in the canonical frame $\boldsymbol{\mu}_0$ as N randomly sampled 3D tracks locations from this set of initial observations. We then perform k-means clustering on the vectorized velocities of the noisy 3D tracks $\{\mathbf{X}_t\}$, and initialize the motion bases $\{\mathbf{T}_{0 \rightarrow t}^{(b)}\}_{b=1}^B$ from these B clusters of tracks. Specifically, for the set of trajectories $\{\mathbf{X}_t\}_b$ belonging to cluster b , we initialize the basis transform $\mathbf{T}_{0 \rightarrow \tau}^{(b)}$ using weighted Procrustes alignment between the point sets $\{\mathbf{X}_0\}_b$ and $\{\mathbf{X}_\tau\}_b$ for all $\tau = 0, \dots, T$, where the weights are computed using uncertainty and visibility scores from TAPIR predictions. We initialize $\mathbf{w}^{(b)}$ of each Gaussian to decay exponentially with its distance from the center of cluster b in the canonical frame. We then optimize $\boldsymbol{\mu}_0$, $\mathbf{w}^{(b)}$, and set of basis functions $\{\mathbf{T}_{0 \rightarrow t}^{(b)}\}_{b=1}^B$ to fit the observed 3D tracks with an ℓ_1 -loss under temporal smoothness constraints.

Training. We supervise the dynamic Gaussians with two sets of losses. The first set of losses comprise our reconstruction loss to match the per-frame pixelwise color, depth, and masks inputs. The second set of losses enforce consistency of correspondences across time. Specifically, during each training step, we render the image $\hat{\mathbf{I}}_t$, depth $\hat{\mathbf{D}}_t$, and mask $\hat{\mathbf{M}}_t$ from their corresponding training cameras $(\mathbf{K}_t, \mathbf{E}_t)$ according to Equation 2. We supervise these predictions with a reconstruction loss applied independently per-frame

$$L_{\text{recon}} = \|\hat{\mathbf{I}} - \mathbf{I}\|_1 + \lambda_{\text{depth}} \|\hat{\mathbf{D}} - \mathbf{D}\|_1 + \lambda_{\text{mask}} \|\hat{\mathbf{M}} - 1\|_1. \quad (7)$$

The second set of losses supervises the motion of the Gaussians between frames. Specifically, we additionally render the 2D tracks $\hat{\mathbf{u}}_{t \rightarrow t'}$ and reprojected depths $\hat{\mathbf{D}}_{t \rightarrow t'}$, for a pair of randomly sampled query time t and target time t' . We supervise these rendered correspondences with the lifted long-range 2D track

estimates via

$$L_{\text{track-2d}} = \|\mathbf{U}_{t \rightarrow t'} - \hat{\mathbf{U}}_{t \rightarrow t'}\|_1, \text{ and } L_{\text{track-depth}} = \|\hat{\mathbf{d}}_{t \rightarrow t'} - \hat{\mathbf{D}}(\mathbf{U}_{t \rightarrow t'})\|_1. \quad (8)$$

Finally, we enforce a distance-preserving loss between randomly sampled dynamic Gaussians and their k-nearest neighbors. Let $\hat{\mathbf{X}}_t$ and $\hat{\mathbf{X}}_{t'}$ denote the location of a Gaussian at time t and t' , and $\mathcal{C}_k(\hat{\mathbf{X}}_t)$ denote the set of k-nearest neighbors of $\hat{\mathbf{X}}_t$, we define

$$L_{\text{rigidity}} = \left\| \text{dist}(\hat{\mathbf{X}}_t, \mathcal{C}_k(\hat{\mathbf{X}}_t)) - \text{dist}(\hat{\mathbf{X}}_{t'}, \mathcal{C}_k(\hat{\mathbf{X}}_{t'})) \right\|_2^2, \quad (9)$$

where $\text{dist}(\cdot, \cdot)$ measures Euclidean distance.

Implementation Details. For in-the-wild videos, we obtain their camera parameters with the following procedure: we first run UniDepth [66] to get the camera intrinsics and metric depth maps, and then run Droid-SLAM [87] in RGB-D mode with UniDepth’s depth maps to obtain the camera poses. This process is efficient and provides accurate camera parameters. For evaluating our methods on public benchmark, we use the camera annotations that come with the datasets (e.g., from COLMAP [77] or simulation).

We optimize our model using Adam Optimizer [41]. We perform 1000 iterations of optimization for the initial fitting and 500 epochs for joint optimization, respectively. The number of $\mathbb{SE}(3)$ bases B is set to 20 for all of our experiments. We initialize 40k dynamic Gaussians for the dynamic part and 100k static Gaussians for the static part of the scene, respectively. We perform the same adaptive Gaussian controls for dynamic and static Gaussians as per 3D-GS [40]. Training on a sequence of 300 frames of 960×720 resolution takes about 2 hours to finish on an A100 GPU. Our rendering FPS is around 40 fps.

4 Experiments

We evaluate our performance quantitatively and qualitatively on a broad range of tasks: long range 3D point tracking, long-range 2D point tracking, and novel view synthesis. We focus our evaluation in particular on datasets that exhibit substantial scene motion. In particular, the iPhone dataset [21] features casual captures of real-world scenes that closely match our target scenarios. It provides comprehensive annotations, including simultaneous validation views, lidar depth, sparse 2D point correspondences across the entire video, and can be used to evaluate our performance on all three tasks. Given the challenge of obtaining precise 3D track annotations for real data, we also evaluate performance using the scenes from the synthetic MOVi-F Kubric dataset [23].

4.1 Task Specification

Long-range 3D tracking. Our primary task is estimating 3D scene motion for any pixel over long period of time (up to over 10 seconds). For this purpose,

Table 1: Evaluation on iPhone dataset. Our method achieves SOTA performance all tasks of 3D point tracking, 2D point tracking, and novel view synthesis. The baselines that perform best on 2D and 3D tracking (TAPIR [14]+DA [106] and CoTracker [38]+DA [106]) are unable to synthesize novel viewpoints of the scene, while the methods that perform best in novel view synthesis (T-NeRF [21] and HyperNeRF [65]) struggle with or fail to produce 2D and 3D tracks. Our method achieves a significant boost in all three tasks above baselines.

Method	3D Tracking			2D Tracking			View Synthesis		
	EPE ↓	δ_{3D}^{05} ↑	δ_{3D}^{10} ↑	AJ ↑	$<\delta_{avg}$ ↑	OA ↑	PSNR ↑	SSIM ↑	LPIPS ↓
T-NeRF [21]	-	-	-	-	-	-	15.60	0.55	0.55
HyperNeRF [65]	0.182	28.4	45.8	10.1	19.3	52.0	15.99	0.59	0.51
DynIBar [52]	0.252	11.4	24.6	5.4	8.7	37.7	13.41	0.48	0.55
Deformable-3D-GS [108]	0.151	33.4	55.3	14.0	20.9	63.9	11.92	0.49	0.66
CoTracker [38]+DA [106]	0.202	34.3	57.9	24.1	33.9	73.0	-	-	-
TAPIR [14]+DA [106]	0.114	38.1	63.2	27.8	41.5	67.4	-	-	-
Ours	0.082	43.0	73.3	34.4	47.0	86.6	16.72	0.63	0.45

we extend the metrics for scene flow evaluation introduced in RAFT-3D [88] to evaluate long-range 3D tracking. Specifically, we report the 3D end-point-error (EPE), which measures the Euclidean distance between the ground truth 3D tracks and predicted tracks at each target time step. In addition, we report the percentage of points that fall within a given threshold of the ground truth 3D location $\delta_{3D}^{05} = 5\text{cm}$ and $\delta_{3D}^{10} = 10\text{cm}$ in metric scale.

Long-range 2D tracking. Our globally consistent 3D motion representation can be easily projected onto image plane to get long-range 2D tracks. We therefore also evaluate 2D tracking performance in terms of both position accuracy and occlusion accuracy following the metrics introduced in the TAP-Vid benchmark [13], and report the Average Jaccard (AJ), average position accuracy ($<\delta_{avg}$), and Occlusion Accuracy (OA).

Novel view synthesis. We measure our method’s novel view synthesis quality as a comprehensive assessment for geometry, appearance, and motion. We evaluate on the iPhone dataset [21] which provides validation views and report co-visibility masked image metrics [21]: mPSNR, mSSIM [96] and mLPIPS [22, 29].

4.2 Baselines

Our method represents dynamic 3D scene comprehensively with explicit long-range 3D scene motion estimation, which also allows for novel view synthesis. While no existing method achieves the exact same goals as ours, there are methods that focus on sub-tasks related to our problem, such as dynamic novel view synthesis, 2D tracking, or monocular depth estimation. We therefore adapt existing methods as our baselines which are introduced below.

While dynamic novel view synthesis approaches focus primarily on the photometric reconstruction quality and do not explicitly output 3D point tracks, we

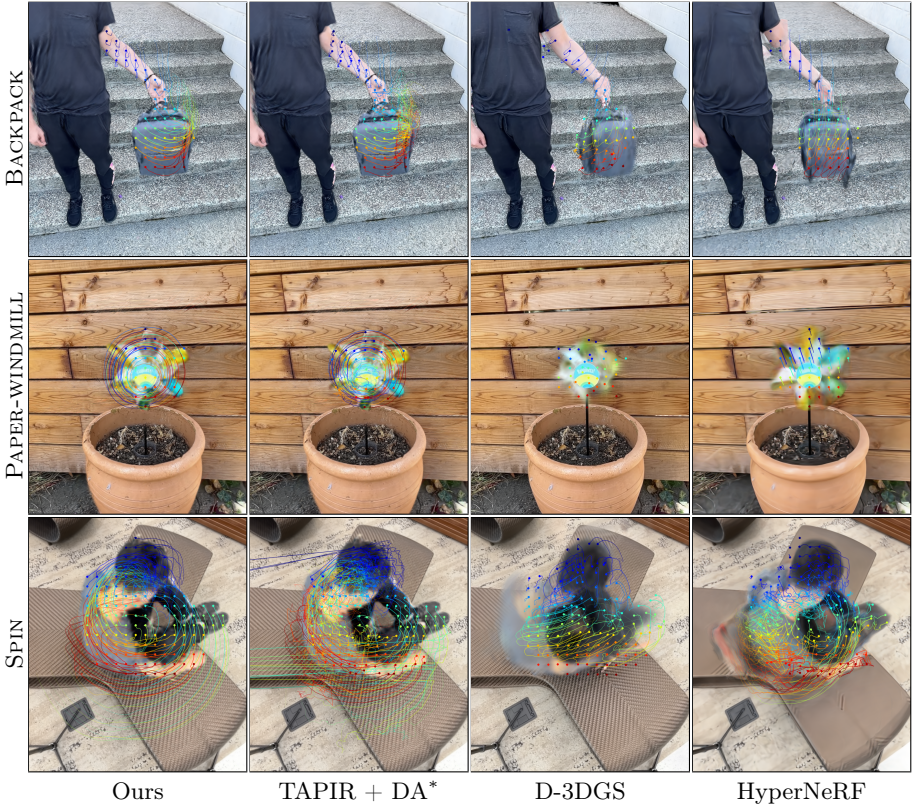


Fig. 3: 3D Track visualization on iPhone dataset. We render novel views for each method and overlay their predicted 3D tracks on top of the rendered images. For clarity, we only display a segment of the entire trails spanning 50 frames for a specific set of grid query points. However, it is important to note that our method can generate dense, full-length 3D tracks. *Note that TAPIR + DA cannot produce novel view rendering, and we overlay their tracking results with our rendering to make it easier to interpret.

can adapt some of their representations to derive 3D point tracks for our evaluation. For HyperNeRF [65], we compose the learned inverse mapping (from view space to canonical space) and a forward mapping solved via root-finding [11, 21] to produce 3D tracks at query points. DynIBaR [52] produces short-range view-to-view scene flow, which we chain into long-range 3D tracks for our evaluation. Deformable-3D-GS (D-3DGS) [108] represents dynamic scenes using 3D Gaussians [39] in the canonical space and a deformation MLP network that deforms the canonical 3D Gaussians into each view, which naturally allows 3D motion computation. Finally, T-NeRF [21] models dynamic scenes using time as MLP input in addition to 3D locations, which does not provide a method for extracting 3D motion, and hence they are not considered for 2D/3D tracking evaluation.



Fig. 4: Qualitative comparison of novel-view synthesis on iPhone dataset. The leftmost image in each row shows the training view at the same time step as the validation view. The regions highlighted in green indicate areas excluded from evaluation due to the lack of co-visibility between training and validation views.

We evaluate the 3D tracks of these methods only on the iPhone dataset, because we found none can handle the Kubric scene motion.

In addition to dynamic view synthesis baselines, we would also like to include baselines that focus on estimating 3D tracks. However, we did not find prior work that produces long-range 3D tracks from generic monocular videos, hence we adapt existing SOTA methods for long-range 2D tracking and monocular depth estimation. Specifically, we take the state-of-art long-range 2D tracks from TAPIR [14] and CoTracker [38] and lift them into 3D scene motion using monocular depth maps produced by Depth Anything (DA) [106]. We compute the correct scale and shift for each relative depth map from Depth Anything to align them with the scene. The two resulting baselines are called “CoTracker [38] + DA [106]” and “TAPIR [14] + DA [106]”. Note that these baselines can only produce 3D tracks for visible regions, as the depth values for occluded points are unknown from such a 2.5D representation. In contrast, our global representation allows for modeling 3D motion through occlusions.

4.3 Evaluation on iPhone Dataset

iPhone dataset [21] contains 14 sequences of 200-500 frames featuring various types of challenging real world scene motion. All sequences are recorded using a handheld moving camera in a casual manner, with 7 of them additionally featuring two synchronized static cameras with a large baseline for novel view synthesis evaluation. It also comes with metric depth from the lidar sensors and annotations of 5 to 15 keypoints at ten equally spaced time steps for each

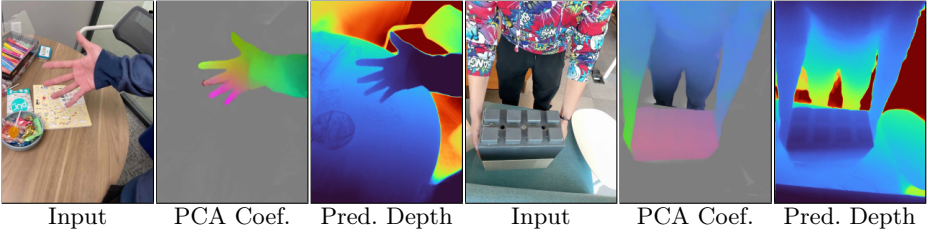


Fig. 5: Visualization of motion coefficients after PCA and predicted depth maps on iPhone dataset. The motion coefficients encode information regarding rigid moving components. For instance, our motion coefficient PCA produces constant color for the block in the second example which exhibits rigid motion.

sequence. For 3D tracking evaluation, we generate the groundtruth 3D tracks by lifting the 2D keypoint annotations into 3D using lidar depth, and masking out points that are occluded or with invalid lidar depth values.

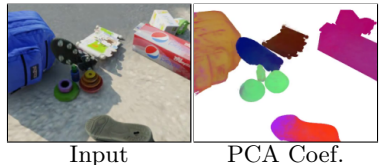
All experiments are conducted with the original instead of half resolution as in [21] given that our method can handle high-res video input. We also discard SPACE-OUT and WHEEL scenes due to camera and lidar error. We find that the original camera annotations from ARKit is not accurate enough, and refine them using global bundle adjustment from COLMAP [78].

We report the quantitative comparison in Tab. 1 which shows that our method outperforms all baselines on all tasks by a substantial margin. On 3D and 2D tracking, we show clear improvement over naive baselines of 2D tracks plus depth maps, and significant improvement over all novel view synthesis methods, e.g., nearly halving the EPE of the second best method Deformable-3D-GS [108]. Our method also achieves the best novel view synthesis quality across dynamic NeRF, IBR, and 3D-GS-based baselines.

Fig. 3 shows qualitative comparison of the 3D tracking results. To illustrate 3D tracking quality, we render the novel views and plot the predicted 3D tracks of the given query points onto the novel views. Since “TAPIR + DA” cannot perform novel view synthesis, we overlay their track predictions onto our renderings to aid interpretation. D-3DGS [108] and HyperNeRF [65] fail to capture the significant scene motion in the paper-windmill and spin sequence, resulting in structure degradation and blurry rendering. “TAPIR + DA” can track large motions, but their 3D tracks tend to be noisy and erroneous. In contrast, our method not only generates the highest-quality novel views but also the most smooth and accurate 3D tracks. Fig. 4 provides additional novel view synthesis comparison on the validation views. In Fig. 5, we provide additional visualization of the outputs from our representation. We visualize the rendering of the first three components of PCA decomposition for the motion coefficients, which correlates well with the rigid groups of the moving object.

Table 2: 3D Tracking evaluation on Kubric dataset.

Method	EPE↓ $\delta_{3D}^{0.05}$ ↑ $\delta_{3D}^{1.0}$ ↑		
CoTracker [38]+DA [106]	0.19	34.4	56.5
TAPIR [14]+DA [106]	0.20	34.0	56.2
Ours	0.16	39.8	62.2

**Fig. 6: First three PCA components of the optimized motion coefficients.**

4.4 Evaluation on the Kubric dataset

The Kubric MOVi-F dataset contains short 24-frame videos of scenes of 10-20 objects, rendered with linear camera movement and motion blur. Multiple rigid objects are tossed onto the scene, at a speed that far exceeds the speed of the moving camera, making it a similar capture scenario to in-the-wild capture scenarios. It provides dense comprehensive annotations, including ground truth depth maps, camera parameters, segmentation masks, and point correspondences that are dense across time. We use 30 scenes from the MOVi-F validation set to evaluate the accuracy of our long-range 3D point tracks for all points in time.

We demonstrate our method on the synthetic Kubric MOVi-F dataset in long-range 3D point tracking across time. Of the above baselines, only “CoTracker [38]+DA [106]” and “TAPIR [38]+DA [106]” yield 3D tracks for these scenes. For all baselines, we provide the ground truth camera intrinsics and extrinsics, and monocular depth estimates that have been aligned to the ground truth depth map. We obtain point tracks for all non-background pixels for each method.

We report our quantitative 3D point tracking metrics in Table 2, and find that across all metrics, our method outperforms the baselines. Moreover, we find qualitatively that the optimized motion coefficients of the scene representation are coherently grouped with each moving object in the scene. We demonstrate this in Figure 6, where we show the first 3 PCA components of our optimized motion coefficients of evaluation scenes.

4.5 Ablation studies

We ablate various components of our method on the iPhone dataset in 3D tracking in Table 3. We first validate our choices of motion representation, namely the $\mathbb{SE}(3)$ motion bases parameterization, with two ablations: 1) “Per-Gaussian Transl.”: replacing our motion representation with naive per-Gaussian translational motion trajectories, and 2) “Transl Bases.”: keeping the motion bases representation but only using translational bases instead of $\mathbb{SE}(3)$. We find $\mathbb{SE}(3)$ bases lead to a noticeable improvement in 3D tracking compared to both translational bases and per-Gaussian translational motion representation.

Next, we ablate our training strategies including initialization and supervision signal. We conduct an ablation of “No $\mathbb{SE}(3)$ Init.”, where instead of performing our initial $\mathbb{SE}(3)$ fitting stage, we initialize the translational part of the

Table 3: Ablation Studies on iPhone dataset.

Methods	$\mathbb{SE}(3)$	Motion Basis	2D tracks	Initialization	EPE↓	$\delta_{3D}^{05} \uparrow$	$\delta_{3D}^{10} \uparrow$
Ours (Full)	✓	✓	✓	✓	0.082	43.0	73.3
Transl. Bases		✓	✓	✓	0.093	42.3	69.9
Per-Gaussian Transl.			✓	✓	0.087	41.2	69.2
No $\mathbb{SE}(3)$ Init.	✓	✓	✓		0.111	39.3	65.7
No 2D Tracks	✓	✓			0.141	30.4	57.8

motion bases with randomly selected noisy 3D tracks formed by directly lifting input 2D tracks using depth maps into 3D, and the rotation part as identity. We find that skipping this initialization noticeably hurts performance. Lastly, we remove the 2D track supervision entirely (“No 2D Tracks”) and find it to lead to significant drop in performance, which verifies the importance of the 2D track supervision for 3D tracking.

5 Discussion and Conclusion

Limitations. Although our approach demonstrates promising steps towards long-range 3D tracking and accurate reconstruction of complex 3D dynamic scenes, several limitations remain. Similar to most prior monocular dynamic view synthesis methods, our system still requires per-scene test-time optimization, which hinders its use in streamable applications. In addition, it cannot handle large changes in camera viewpoint, which require some kind of generative capabilities or data-driven priors to hallucinate unseen regions. Moreover, our approach relies on accurate camera parameters obtained from off-the-shelf algorithms, suggesting potential failure in scenes dominated by texture-less regions or moving objects. Finally, our method relies on user input to generate the mask of moving objects. A promising research direction would be to design a feed-forward network approach for jointly estimating camera poses, scene geometry, and motion trajectories from an unconstrained monocular video.

Please note that since we wrote this paper, there have been several concurrent works posted on arXiv [46, 54, 82, 95] that also address this setup of monocular 4D reconstruction from causal videos. As far as we know, all of them are optimization-based approaches, also utilizing strong off-the-shelf data-driven priors. We leave it to future work to compare these approaches.

Conclusion. We presented a new method for joint long-range 3D tracking and novel view synthesis from dynamic scene captured by a monocular video. Our approach models dense dynamic scene elements with a global set of 3D Gaussians that translate and rotate over time. We regularize the full-length 3D motion trajectories of each Gaussian, ensuring smoothness and low dimensionality, by parameterizing them as linear combinations of a compact set of rigid motion bases. To overcome the ill-posed nature of this problem in monocular capture settings, we further design the model to regularize by consolidating noisy data-driven

observations into a globally consistent estimate of scene appearance, geometry, and motion. Extensive evaluations on both synthetic and real benchmarks demonstrate that our approach significantly improves upon prior state-of-the-art methods in both 2D/3D long-range tracking and novel view synthesis tasks.

Acknowledgement. We thank Ruilong Li, Noah Snavely, Brent Yi and Aleksander Holynski for helpful discussion. This project is supported in part by DARPA No. HR001123C0021. and IARPA DOI/IBC No. 140D0423C0035. The views and conclusions contained herein are those of the authors and do not represent the official policies or endorsements of these institutions.

References

1. Bansal, A., Vo, M., Sheikh, Y., Ramanan, D., Narasimhan, S.: 4d visualization of dynamic events from unconstrained multi-view videos. In: Proceedings of the IEEE/CVF Conference on Computer Vision and Pattern Recognition. pp. 5366–5375 (2020) [3](#)
2. Bay, H., Tuytelaars, T., Gool, L.V.: Surf: Speeded up robust features. In: European Conference on Computer Vision (2006) [3](#)
3. Birchfield, S.T., Pundlik, S.J.: Joint tracking of features and edges. In: 2008 IEEE Conference on Computer Vision and Pattern Recognition. pp. 1–6. IEEE (2008) [3](#)
4. Black, M.J., Anandan, P.: A framework for the robust estimation of optical flow. In: 1993 (4th) International Conference on Computer Vision. pp. 231–236. IEEE (1993) [3](#)
5. Bozic, A., Zollhöfer, M., Theobalt, C., Nießner, M.: Deepdeform: Learning non-rigid rgb-d reconstruction with semi-supervised data. 2020 IEEE/CVF Conference on Computer Vision and Pattern Recognition (CVPR) pp. 7000–7010 (2019) [3](#)
6. Brox, T., Bregler, C., Malik, J.: Large displacement optical flow. 2009 IEEE Conference on Computer Vision and Pattern Recognition pp. 41–48 (2009) [3](#)
7. Brox, T., Bruhn, A., Papenberger, N., Weickert, J.: High accuracy optical flow estimation based on a theory for warping. In: European Conference on Computer Vision (2004) [3](#)
8. Broxton, M., Flynn, J., Overbeck, R., Erickson, D., Hedman, P., Duvall, M., Dourgarian, J., Busch, J., Whalen, M., Debevec, P.: Immersive light field video with a layered mesh representation. ACM Transactions on Graphics (TOG) **39**(4), 86–1 (2020) [1](#), [3](#)
9. Bruhn, A., Weickert, J., Schnörr, C.: Lucas/kanade meets horn/schunck: Combining local and global optic flow methods. International journal of computer vision **61**, 211–231 (2005) [3](#)
10. Cao, A., Johnson, J.: Hexplane: A fast representation for dynamic scenes. In: Proceedings of the IEEE/CVF Conference on Computer Vision and Pattern Recognition. pp. 130–141 (2023) [3](#)
11. Chen, X., Zheng, Y., Black, M.J., Hilliges, O., Geiger, A.: Snarf: Differentiable forward skinning for animating non-rigid neural implicit shapes. In: Proceedings of the IEEE/CVF International Conference on Computer Vision. pp. 11594–11604 (2021) [10](#)

12. DeTone, D., Malisiewicz, T., Rabinovich, A.: Superpoint: Self-supervised interest point detection and description. 2018 IEEE/CVF Conference on Computer Vision and Pattern Recognition Workshops (CVPRW) pp. 337–33712 (2017) [3](#)
13. Doersch, C., Gupta, A., Markeeva, L., Recasens, A., Smaira, L., Aytar, Y., Carreira, J., Zisserman, A., Yang, Y.: Tap-vid: A benchmark for tracking any point in a video. *Advances in Neural Information Processing Systems* **35**, 13610–13626 (2022) [3](#), [9](#)
14. Doersch, C., Yang, Y., Vecerik, M., Gokay, D., Gupta, A., Aytar, Y., Carreira, J., Zisserman, A.: Tapir: Tracking any point with per-frame initialization and temporal refinement. *arXiv preprint arXiv:2306.08637* (2023) [3](#), [4](#), [7](#), [9](#), [11](#), [13](#)
15. Dosovitskiy, A., Fischer, P., Ilg, E., Häusser, P., Hazirbas, C., Golkov, V., van der Smagt, P., Cremers, D., Brox, T.: FlowNet: Learning optical flow with convolutional networks. 2015 IEEE International Conference on Computer Vision (ICCV) pp. 2758–2766 (2015) [3](#)
16. Dou, M., Khamis, S., Degtyarev, Y., Davidson, P.L., Fanello, S., Kowdle, A., Orts, S., Rhemann, C., Kim, D., Taylor, J., Kohli, P., Tankovich, V., Izadi, S.: Fusion4d. *ACM Transactions on Graphics (TOG)* **35**, 1 – 13 (2016) [3](#)
17. Du, Y., Zhang, Y., Yu, H.X., Tenenbaum, J.B., Wu, J.: Neural radiance flow for 4d view synthesis and video processing. In: 2021 IEEE/CVF International Conference on Computer Vision (ICCV). pp. 14304–14314. IEEE Computer Society (2021) [3](#)
18. Duan, Y., Wei, F., Dai, Q., He, Y., Chen, W., Chen, B.: 4d gaussian splatting: Towards efficient novel view synthesis for dynamic scenes. *arXiv preprint arXiv:2402.03307* (2024) [3](#)
19. Fridovich-Keil, S., Meanti, G., Warburg, F.R., Recht, B., Kanazawa, A.: K-planes: Explicit radiance fields in space, time, and appearance. In: *Proceedings of the IEEE/CVF Conference on Computer Vision and Pattern Recognition*. pp. 12479–12488 (2023) [1](#), [3](#)
20. Gao, C., Saraf, A., Kopf, J., Huang, J.B.: Dynamic view synthesis from dynamic monocular video. In: *Proceedings of the IEEE International Conference on Computer Vision* (2021) [2](#)
21. Gao, H., Li, R., Tulsiani, S., Russell, B., Kanazawa, A.: Dynamic novel-view synthesis: A reality check. In: *NeurIPS* (2022) [3](#), [4](#), [8](#), [9](#), [10](#), [11](#), [12](#)
22. Gatys, L.A., Ecker, A.S., Bethge, M., Hertzmann, A., Shechtman, E.: Controlling perceptual factors in neural style transfer. In: *Proceedings of the IEEE conference on computer vision and pattern recognition*. pp. 3985–3993 (2017) [9](#)
23. Greff, K., Belletti, F., Beyer, L., Doersch, C., Du, Y., Duckworth, D., Fleet, D.J., Gnanaprasam, D., Golemo, F., Herrmann, C., et al.: Kubric: A scalable dataset generator. In: *Proceedings of the IEEE/CVF Conference on Computer Vision and Pattern Recognition*. pp. 3749–3761 (2022) [8](#)
24. Gu, X., Wang, Y., Wu, C., Lee, Y.J., Wang, P.: HplflowNet: Hierarchical permutohedral lattice flowNet for scene flow estimation on large-scale point clouds. 2019 IEEE/CVF Conference on Computer Vision and Pattern Recognition (CVPR) pp. 3249–3258 (2019) [1](#), [3](#)
25. Harley, A.W., Fang, Z., Fragkiadaki, K.: Particle video revisited: Tracking through occlusions using point trajectories. In: *European Conference on Computer Vision*. pp. 59–75. Springer (2022) [3](#)
26. Hempel, T., Abdelrahman, A.A., Al-Hamadi, A.: 6d rotation representation for unconstrained head pose estimation. In: 2022 IEEE International Conference on Image Processing (ICIP). pp. 2496–2500. IEEE (2022) [6](#)

27. Horn, B.K.P., Schunck, B.G.: Determining optical flow. In: Other Conferences (1981) **3**
28. Huang, Z., Shi, X., Zhang, C., Wang, Q., Cheung, K.C., Qin, H., Dai, J., Li, H.: Flowformer: A transformer architecture for optical flow. In: European Conference on Computer Vision. pp. 668–685. Springer (2022) **3**
29. Huh, M., Zhang, R., Zhu, J.Y., Paris, S., Hertzmann, A.: Transforming and projecting images into class-conditional generative networks. In: Computer Vision—ECCV 2020: 16th European Conference, Glasgow, UK, August 23–28, 2020, Proceedings, Part II 16. pp. 17–34. Springer (2020) **9**
30. Hur, J., Roth, S.: Self-supervised monocular scene flow estimation. 2020 IEEE/CVF Conference on Computer Vision and Pattern Recognition (CVPR) pp. 7394–7403 (2020) **3**
31. Ilg, E., Mayer, N., Saikia, T., Keuper, M., Dosovitskiy, A., Brox, T.: FlowNet 2.0: Evolution of optical flow estimation with deep networks. In: Proceedings of the IEEE conference on computer vision and pattern recognition. pp. 2462–2470 (2017) **3**
32. Innmann, M., Zollhöfer, M., Nießner, M., Theobalt, C., Stamminger, M.: Volumedeform: Real-time volumetric non-rigid reconstruction. In: European Conference on Computer Vision (2016) **3**
33. Işık, M., Rünz, M., Georgopoulos, M., Khakhulin, T., Starck, J., Agapito, L., Nießner, M.: Humanrf: High-fidelity neural radiance fields for humans in motion. arXiv preprint arXiv:2305.06356 (2023) **3**
34. Jaimes, M., Souiai, M., Jiménez, J.G., Cremers, D.: A primal-dual framework for real-time dense rgb-d scene flow. 2015 IEEE International Conference on Robotics and Automation (ICRA) pp. 98–104 (2015), <https://api.semanticscholar.org/CorpusID:16757067> **3**
35. Janai, J., Guney, F., Ranjan, A., Black, M., Geiger, A.: Unsupervised learning of multi-frame optical flow with occlusions. In: Proceedings of the European conference on computer vision (ECCV). pp. 690–706 (2018) **3**
36. Jiang, S., Campbell, D., Lu, Y., Li, H., Hartley, R.: Learning to estimate hidden motions with global motion aggregation. In: Proceedings of the IEEE/CVF International Conference on Computer Vision. pp. 9772–9781 (2021) **3**
37. Jiang, S., Lu, Y., Li, H., Hartley, R.: Learning optical flow from a few matches. In: Proceedings of the IEEE/CVF conference on computer vision and pattern recognition. pp. 16592–16600 (2021) **3**
38. Karaev, N., Rocco, I., Graham, B., Neverova, N., Vedaldi, A., Rupprecht, C.: CoTracker: It is better to track together (2023) **3, 9, 11, 13**
39. Kerbl, B., Kopanas, G., Leimkühler, T., Drettakis, G.: 3d gaussian splatting for real-time radiance field rendering. ACM Transactions on Graphics **42**(4) (2023) **1, 5, 10**
40. Kerbl, B., Kopanas, G., Leimkühler, T., Drettakis, G.: 3d gaussian splatting for real-time radiance field rendering. ACM Transactions on Graphics **42**(4) (July 2023), <https://repo-sam.inria.fr/fungraph/3d-gaussian-splatting/> **3, 8**
41. Kingma, D.P., Ba, J.A., Adam, J.: A method for stochastic optimization. arxiv 2014. arXiv preprint arXiv:1412.6980 **106** (2020) **8**
42. Kirillov, A., Mintun, E., Ravi, N., Mao, H., Rolland, C., Gustafson, L., Xiao, T., Whitehead, S., Berg, A.C., Lo, W.Y., Dollár, P., Girshick, R.B.: Segment anything. 2023 IEEE/CVF International Conference on Computer Vision (ICCV) pp. 3992–4003 (2023) **7**

43. Kopf, J., Rong, X., Huang, J.B.: Robust consistent video depth estimation. In: Proceedings of the IEEE/CVF Conference on Computer Vision and Pattern Recognition. pp. 1611–1621 (2021) [3](#)
44. Kratimenos, A., Lei, J., Daniilidis, K.: Dynmf: Neural motion factorization for real-time dynamic view synthesis with 3d gaussian splatting. arXiv (2023) [4](#), [6](#)
45. Kumar, S., Dai, Y., Li, H.: Monocular dense 3d reconstruction of a complex dynamic scene from two perspective frames. 2017 IEEE International Conference on Computer Vision (ICCV) pp. 4659–4667 (2017) [3](#)
46. Lei, J., Weng, Y., Harley, A., Guibas, L., Daniilidis, K.: Mosca: Dynamic gaussian fusion from casual videos via 4d motion scaffolds. arXiv preprint arXiv:2405.17421 (2024) [14](#)
47. Li, R., Tanke, J., Vo, M., Zollhöfer, M., Gall, J., Kanazawa, A., Lassner, C.: Tava: Template-free animatable volumetric actors. In: European Conference on Computer Vision. pp. 419–436. Springer (2022) [3](#)
48. Li, T., Slavcheva, M., Zollhoefer, M., Green, S., Lassner, C., Kim, C., Schmidt, T., Lovegrove, S., Goesele, M., Newcombe, R., et al.: Neural 3d video synthesis from multi-view video. In: Proceedings of the IEEE/CVF Conference on Computer Vision and Pattern Recognition. pp. 5521–5531 (2022) [3](#)
49. Li, Z., Chen, Z., Li, Z., Xu, Y.: Spacetime gaussian feature splatting for real-time dynamic view synthesis. arXiv preprint arXiv:2312.16812 (2023) [3](#)
50. Li, Z., Dekel, T., Cole, F., Tucker, R., Snavely, N., Liu, C., Freeman, W.T.: Learning the depths of moving people by watching frozen people. In: Proceedings of the IEEE/CVF conference on computer vision and pattern recognition. pp. 4521–4530 (2019) [3](#), [4](#)
51. Li, Z., Niklaus, S., Snavely, N., Wang, O.: Neural scene flow fields for space-time view synthesis of dynamic scenes. In: Proceedings of the IEEE/CVF Conference on Computer Vision and Pattern Recognition. pp. 6498–6508 (2021) [2](#), [3](#)
52. Li, Z., Wang, Q., Cole, F., Tucker, R., Snavely, N.: Dynibar: Neural dynamic image-based rendering. In: Proceedings of the IEEE/CVF Conference on Computer Vision and Pattern Recognition. pp. 4273–4284 (2023) [2](#), [3](#), [4](#), [9](#), [10](#)
53. Liu, C., Yuen, J., Torralba, A.: Sift flow: Dense correspondence across scenes and its applications. IEEE Transactions on Pattern Analysis and Machine Intelligence **33**, 978–994 (2011) [3](#)
54. Liu, Q., Liu, Y., Wang, J., Lv, X., Wang, P., Wang, W., Hou, J.: Modgs: Dynamic gaussian splatting from causually-captured monocular videos. arXiv preprint arXiv:2406.00434 (2024) [14](#)
55. Liu, X., Qi, C., Guibas, L.J.: Learning scene flow in 3d point clouds. ArXiv **abs/1806.01411** (2018) [1](#), [3](#)
56. Lowe, D.G.: Distinctive image features from scale-invariant keypoints. International Journal of Computer Vision **60**, 91–110 (2004) [3](#)
57. Lucas, B.D., Kanade, T.: An iterative image registration technique with an application to stereo vision. In: International Joint Conference on Artificial Intelligence (1981) [3](#)
58. Luiten, J., Kopanas, G., Leibe, B., Ramanan, D.: Dynamic 3d gaussians: Tracking by persistent dynamic view synthesis. ArXiv **abs/2308.09713** (2023) [1](#)
59. Luo, X., Huang, J.B., Szeliski, R., Matzen, K., Kopf, J.: Consistent video depth estimation. ACM Transactions on Graphics (ToG) **39**(4), 71–1 (2020) [3](#)
60. Mehl, L., Jahedi, A., Schmalfluss, J., Bruhn, A.: M-fuse: Multi-frame fusion for scene flow estimation. In: Proceedings of the IEEE/CVF Winter Conference on Applications of Computer Vision. pp. 2020–2029 (2023) [3](#)

61. Mildenhall, B., Srinivasan, P.P., Tancik, M., Barron, J.T., Ramamoorthi, R., Ng, R.: Nerf: Representing scenes as neural radiance fields for view synthesis. In: ECCV (2020) **1**, **3**
62. Neoral, M., Šerých, J., Matas, J.: Mft: Long-term tracking of every pixel. In: Proceedings of the IEEE/CVF Winter Conference on Applications of Computer Vision (WACV). pp. 6837–6847 (January 2024) **3**
63. Newcombe, R.A., Fox, D., Seitz, S.M.: Dynamicfusion: Reconstruction and tracking of non-rigid scenes in real-time. 2015 IEEE Conference on Computer Vision and Pattern Recognition (CVPR) pp. 343–352 (2015) **3**
64. Park, K., Sinha, U., Barron, J.T., Bouaziz, S., Goldman, D.B., Seitz, S.M., Martin-Brualla, R.: Nerfies: Deformable neural radiance fields. In: Proceedings of the IEEE/CVF International Conference on Computer Vision. pp. 5865–5874 (2021) **2**, **3**
65. Park, K., Sinha, U., Hedman, P., Barron, J.T., Bouaziz, S., Goldman, D.B., Martin-Brualla, R., Seitz, S.M.: Hypernerf: A higher-dimensional representation for topologically varying neural radiance fields. arXiv preprint arXiv:2106.13228 (2021) **2**, **3**, **9**, **10**, **12**
66. Piccinelli, L., Yang, Y.H., Sakaridis, C., Segu, M., Li, S., Van Gool, L., Yu, F.: UniDepth: Universal monocular metric depth estimation. In: Proceedings of the IEEE/CVF Conference on Computer Vision and Pattern Recognition (CVPR) (2024) **8**
67. Pumarola, A., Corona, E., Pons-Moll, G., Moreno-Noguer, F.: D-nerf: Neural radiance fields for dynamic scenes. In: Proceedings of the IEEE/CVF Conference on Computer Vision and Pattern Recognition. pp. 10318–10327 (2021) **3**
68. Puy, G., Boulch, A., Marlet, R.: Flot: Scene flow on point clouds guided by optimal transport. In: European Conference on Computer Vision (2020) **1**, **3**
69. Quiroga, J., Brox, T., Devernay, F., Crowley, J.L.: Dense semi-rigid scene flow estimation from rgbd images. In: European Conference on Computer Vision (2014), <https://api.semanticscholar.org/CorpusID:10240196> **3**
70. Ranftl, R., Vineet, V., Chen, Q., Koltun, V.: Dense monocular depth estimation in complex dynamic scenes. In: Proceedings of the IEEE Conference on Computer Vision and Pattern Recognition (CVPR) (June 2016) **3**
71. Ren, Z., Gallo, O., Sun, D., Yang, M.H., Sudderth, E.B., Kautz, J.: A fusion approach for multi-frame optical flow estimation. In: 2019 IEEE Winter Conference on Applications of Computer Vision (WACV). pp. 2077–2086. IEEE (2019) **3**
72. Rubinstein, M., Liu, C.: Towards longer long-range motion trajectories. In: British Machine Vision Conference (2012) **3**
73. Rublee, E., Rabaud, V., Konolige, K., Bradski, G.R.: Orb: An efficient alternative to sift or surf. 2011 International Conference on Computer Vision pp. 2564–2571 (2011) **3**
74. Russell, C., Yu, R., Agapito, L.: Video pop-up: Monocular 3d reconstruction of dynamic scenes. In: European conference on computer vision. pp. 583–598. Springer (2014) **3**
75. Sand, P.: Long-range video motion estimation using point trajectories. Ph.D. thesis, Ph. D. dissertation, Cambridge, MA, USA, 2006, adviser-Teller, Seth **3**
76. Sand, P., Teller, S.: Particle video: Long-range motion estimation using point trajectories. International journal of computer vision **80**, 72–91 (2008) **3**
77. Schonberger, J.L., Frahm, J.M.: Structure-from-motion revisited. In: Proceedings of the IEEE conference on computer vision and pattern recognition. pp. 4104–4113 (2016) **8**

78. Schönberger, J.L., Frahm, J.M.: Structure-from-motion revisited. In: Conference on Computer Vision and Pattern Recognition (CVPR) (2016) [12](#)
79. Shi, X., Huang, Z., Bian, W., Li, D., Zhang, M., Cheung, K.C., See, S., Qin, H., Dai, J., Li, H.: Videoflow: Exploiting temporal cues for multi-frame optical flow estimation. arXiv preprint arXiv:2303.08340 (2023) [3](#)
80. Sivic, J., Schaffalitzky, F., Zisserman, A.: Object level grouping for video shots. *International Journal of Computer Vision* **67**, 189–210 (2004) [3](#)
81. Song, L., Chen, A., Li, Z., Chen, Z., Chen, L., Yuan, J., Xu, Y., Geiger, A.: Nerfplayer: A streamable dynamic scene representation with decomposed neural radiance fields. *IEEE Transactions on Visualization and Computer Graphics* **29**(5), 2732–2742 (2023) [3](#)
82. Stearns, C., Harley, A., Uy, M., Dubost, F., Tombari, F., Wetzstein, G., Guibas, L.: Dynamic gaussian marbles for novel view synthesis of casual monocular videos. arXiv preprint arXiv:2406.18717 (2024) [14](#)
83. Stich, T., Linz, C., Albuquerque, G., Magnor, M.: View and time interpolation in image space. In: *Computer Graphics Forum*. vol. 27, pp. 1781–1787. Wiley Online Library (2008) [3](#)
84. Sun, D., Sudderth, E.B., Pfister, H.: Layered rgb-d scene flow estimation. 2015 IEEE Conference on Computer Vision and Pattern Recognition (CVPR) pp. 548–556 (2015) [3](#)
85. Sun, D., Yang, X., Liu, M.Y., Kautz, J.: Pwc-net: Cnns for optical flow using pyramid, warping, and cost volume. 2018 IEEE/CVF Conference on Computer Vision and Pattern Recognition pp. 8934–8943 (2017) [3](#)
86. Teed, Z., Deng, J.: Raft: Recurrent all-pairs field transforms for optical flow. In: *Computer Vision—ECCV 2020: 16th European Conference, Glasgow, UK, August 23–28, 2020, Proceedings, Part II* 16. pp. 402–419. Springer (2020) [3](#)
87. Teed, Z., Deng, J.: Droid-slam: Deep visual slam for monocular, stereo, and rgb-d cameras. *Advances in neural information processing systems* **34**, 16558–16569 (2021) [8](#)
88. Teed, Z., Deng, J.: Raft-3d: Scene flow using rigid-motion embeddings. In: *Proceedings of the IEEE/CVF Conference on Computer Vision and Pattern Recognition (CVPR)* (2021) [3](#), [9](#)
89. Vedula, S., Rander, P., Collins, R., Kanade, T.: Three-dimensional scene flow. *IEEE transactions on pattern analysis and machine intelligence* **27**(3), 475–480 (2005) [3](#)
90. Wang, C., Eckart, B., Lucey, S., Gallo, O.: Neural trajectory fields for dynamic novel view synthesis. arXiv preprint arXiv:2105.05994 (2021) [3](#), [4](#)
91. Wang, C., Li, X., Pontes, J.K., Lucey, S.: Neural prior for trajectory estimation. 2022 IEEE/CVF Conference on Computer Vision and Pattern Recognition (CVPR) pp. 6522–6532 (2022) [1](#), [3](#)
92. Wang, H., Schmid, C.: Action recognition with improved trajectories. 2013 IEEE International Conference on Computer Vision pp. 3551–3558 (2013) [3](#)
93. Wang, L., Zhang, J., Liu, X., Zhao, F., Zhang, Y., Zhang, Y., Wu, M., Yu, J., Xu, L.: Fourier plenotrees for dynamic radiance field rendering in real-time. In: *Proceedings of the IEEE/CVF Conference on Computer Vision and Pattern Recognition*. pp. 13524–13534 (2022) [3](#)
94. Wang, Q., Chang, Y.Y., Cai, R., Li, Z., Hariharan, B., Holynski, A., Snavely, N.: Tracking everything everywhere all at once. In: *International Conference on Computer Vision* (2023) [3](#), [6](#)
95. Wang, S., Yang, X., Shen, Q., Jiang, Z., Wang, X.: Gflow: Recovering 4d world from monocular video. arXiv preprint arXiv:2405.18426 (2024) [14](#)

96. Wang, Z., Bovik, A.C., Sheikh, H.R., Simoncelli, E.P.: Image quality assessment: from error visibility to structural similarity. *IEEE transactions on image processing* **13**(4), 600–612 (2004) [9](#)
97. Wang, Z., Li, S., Howard-Jenkins, H., Prisacariu, V.A., Chen, M.: Flownet3d++: Geometric losses for deep scene flow estimation. *2020 IEEE Winter Conference on Applications of Computer Vision (WACV)* pp. 91–98 (2019) [1](#), [3](#)
98. Weng, C.Y., Curless, B., Srinivasan, P.P., Barron, J.T., Kemelmacher-Shlizerman, I.: Humannerf: Free-viewpoint rendering of moving people from monocular video. In: *Proceedings of the IEEE/CVF conference on computer vision and pattern recognition*. pp. 16210–16220 (2022) [3](#)
99. Wu, G., Yi, T., Fang, J., Xie, L., Zhang, X., Wei, W., Liu, W., Tian, Q., Wang, X.: 4d gaussian splatting for real-time dynamic scene rendering. *arXiv preprint arXiv:2310.08528* (2023) [1](#), [3](#)
100. Xian, W., Huang, J.B., Kopf, J., Kim, C.: Space-time neural irradiance fields for free-viewpoint video. In: *Proceedings of the IEEE/CVF Conference on Computer Vision and Pattern Recognition*. pp. 9421–9431 (2021) [3](#), [4](#)
101. Xu, H., Zhang, J., Cai, J., Rezatofighi, H., Tao, D.: Gmflow: Learning optical flow via global matching. In: *Proceedings of the IEEE/CVF conference on computer vision and pattern recognition*. pp. 8121–8130 (2022) [3](#)
102. Yang, G., Sun, D., Jampani, V., Vlastic, D., Cole, F., Chang, H., Ramanan, D., Freeman, W.T., Liu, C.: Lasr: Learning articulated shape reconstruction from a monocular video. *2021 IEEE/CVF Conference on Computer Vision and Pattern Recognition (CVPR)* pp. 15975–15984 (2021), <https://api.semanticscholar.org/CorpusID:234093797> [3](#)
103. Yang, G., Sun, D., Jampani, V., Vlastic, D., Cole, F., Liu, C., Ramanan, D.: Viser: Video-specific surface embeddings for articulated 3d shape reconstruction. In: Ranzato, M., Beygelzimer, A., Dauphin, Y., Liang, P., Vaughan, J.W. (eds.) *Advances in Neural Information Processing Systems*. vol. 34, pp. 19326–19338. Curran Associates, Inc. (2021), https://proceedings.neurips.cc/paper_files/paper/2021/file/a11f9e533f28593768ebf87075ab34f2-Paper.pdf [3](#)
104. Yang, G., Vo, M., Neverova, N., Ramanan, D., Vedaldi, A., Joo, H.: Banmo: Building animatable 3d neural models from many casual videos. *2022 IEEE/CVF Conference on Computer Vision and Pattern Recognition (CVPR)* pp. 2853–2863 (2021), <https://api.semanticscholar.org/CorpusID:245425066> [3](#)
105. Yang, J., Gao, M., Li, Z., Gao, S., Wang, F., Zheng, F.: Track anything: Segment anything meets videos (2023) [7](#)
106. Yang, L., Kang, B., Huang, Z., Xu, X., Feng, J., Zhao, H.: Depth anything: Unleashing the power of large-scale unlabeled data. *arXiv:2401.10891* (2024) [4](#), [7](#), [9](#), [11](#), [13](#)
107. Yang, Z., Yang, H., Pan, Z., Zhu, X., Zhang, L.: Real-time photorealistic dynamic scene representation and rendering with 4d gaussian splatting. *arXiv preprint arXiv:2310.10642* (2023) [3](#)
108. Yang, Z., Gao, X., Zhou, W., Jiao, S., Zhang, Y., Jin, X.: Deformable 3d gaussians for high-fidelity monocular dynamic scene reconstruction. *arXiv preprint arXiv:2309.13101* (2023) [2](#), [3](#), [4](#), [9](#), [10](#), [12](#)
109. Yoon, J.S., Kim, K., Gallo, O., Park, H.S., Kautz, J.: Novel view synthesis of dynamic scenes with globally coherent depths from a monocular camera. In: *Proceedings of the IEEE/CVF Conference on Computer Vision and Pattern Recognition*. pp. 5336–5345 (2020) [3](#)

110. Zhang, Z., Cole, F., Li, Z., Rubinstein, M., Snavely, N., Freeman, W.T.: Structure and motion from casual videos. In: European Conference on Computer Vision. pp. 20–37. Springer (2022) [3](#)
111. Zhang, Z., Cole, F., Tucker, R., Freeman, W.T., Dekel, T.: Consistent depth of moving objects in video. *ACM Transactions on Graphics (TOG)* **40**(4), 1–12 (2021) [3](#)
112. Zheng, Y., Harley, A.W., Shen, B., Wetzstein, G., Guibas, L.J.: Pointodyssey: A large-scale synthetic dataset for long-term point tracking. In: Proceedings of the IEEE/CVF International Conference on Computer Vision. pp. 19855–19865 (2023) [3](#)
113. Zollhöfer, M., Nießner, M., Izadi, S., Rhemann, C., Zach, C., Fisher, M., Wu, C., Fitzgibbon, A.W., Loop, C.T., Theobalt, C., Stamminger, M.: Real-time non-rigid reconstruction using an rgb-d camera. *ACM Transactions on Graphics (TOG)* **33**, 1 – 12 (2014) [3](#)